Environmental Chemistry at Vapor/Water Interfaces: Insights from Vibrational Sum Frequency Generation Spectroscopy

Aaron M. Jubb, Wei Hua, and Heather C. Allen

Department of Chemistry, The Ohio State University, Columbus, Ohio 43210; email: ajubb@chemistry.ohio-state.edu, hua.37@buckeyemail.osu.edu, allen@chemistry.ohio-state.edu

Annu. Rev. Phys. Chem. 2012. 63:107–30

First published online as a Review in Advance on January 3, 2012

The *Annual Review of Physical Chemistry* is online at physchem.annualreviews.org

This article's doi: 10.1146/annurev-physchem-032511-143811

0066-426X/12/0505-0107$20.00

Keywords

salts, lipids, atmospheric chemistry, ion binding, oxidation

Abstract

The chemistry that occurs at surfaces has been an intense area of study for many years owing to its complexity and importance in describing a wide range of physical phenomena. The vapor/water interface is particularly interesting from an environmental chemistry perspective as this surface plays host to a wide range of chemistries that influence atmospheric and geochemical interactions. The application of vibrational sum frequency generation (VSFG), an inherently surface-specific, even-order nonlinear optical spectroscopy, enables the direct interrogation of various vapor/aqueous interfaces to elucidate the behavior and reaction of chemical species within the surface regime. In this review we discuss the application of VSFG to the study of a variety of atmospherically important systems at the vapor/aqueous interface. Chemical systems presented include inorganic ionic solutions prevalent in aqueous marine aerosols, small molecular solutes, and long-chain fatty acids relevant to fat-coated aerosols. The ability of VSFG to probe both the organization and reactions that may occur for these systems is highlighted. A future perspective toward the application of VSFG to the study of environmental interfaces is also provided.

1. INTRODUCTION

Interface: any region between two bulk isotropic media that lacks an inversion center, not just the surface

Aerosol: suspended atmospheric particulate matter

VSFG: vibrational sum frequency generation

Beam polarization: the direction, perpendicular or parallel, of the electric field relative to the incident plane for the associated input or output beam

The chemistry that occurs at and near environmental interfaces is responsible for a host of important naturally occurring physical phenomena. Examples include transport across biological membranes (1–3), the mobility and fate of aquatic chemical species in the environment (4, 5), and growth and uptake of atmospheric particulate matter (aerosols) (6). As such, the elucidation of environmental interfacial processes has been the goal of many diverse and thorough experimental and theoretical studies; however, a complete understanding of the chemical organization and dynamics that occur for many two-dimensional interfacial regimes is lacking. The advancement of inherently surface-specific nonlinear optical spectroscopies such as second harmonic generation (SHG) spectroscopy and vibrational sum frequency generation (VSFG) spectroscopy allows for the direct interrogation of molecules lacking an inversion center, which naturally occurs at the interface between two bulk isotropic media such as air and water (7–11). The ability to selectively probe interfacial molecules and provide molecular-level information makes techniques such as VSFG powerful tools for the study of interfacial processes. As such, studies utilizing VSFG, along with accompanying theoretical work, have provided much insight into the behavior of molecules at interfaces (10, 12–25).

Although a complete description of VSFG theory is beyond the scope of this review and has been presented elsewhere (21, 26–29), a brief discussion on VSFG theory is necessary for clarity. Conventional VSFG intensity is proportional to the square modulus of the effective second-order nonlinear susceptibility $|\chi_{eff}^{(2)}|^2$ multiplied by the intensities of the input visible and infrared beams:

$$I_{\mathrm{SFG}} \propto \left|\chi_{eff}^{(2)}\right|^2 I_{\mathrm{vis}} I_{\mathrm{IR}} \propto \left|\chi_{eff,\mathrm{NR}}^{(2)} + \sum_{v} \chi_{eff,v}^{(2)}\right|^2 I_{\mathrm{vis}} I_{\mathrm{IR}}. \quad (1)$$

Here I_{SFG}, I_{vis}, and I_{IR} are the intensities of the output sum frequency beam, the visible excitation beam, and the infrared excitation beam, respectively, and $\chi_{eff,\mathrm{NR}}^{(2)}$ and $\chi_{eff,v}^{(2)}$ refer to the effective nonresonant and resonant components of the second-order nonlinear susceptibility. $\chi_{eff}^{(2)}$ depends on the VSFG experimental setup (i.e., input beam geometry and polarization); most experiments utilize the four most-common beam polarizations: ssp, sps, pss, and ppp, where the first letter corresponds to the output VSFG beam, the second letter corresponds to the input visible beam, and the last letter corresponds to the input infrared beam, with the ssp combination being the most widely utilized. For these polarization combinations, the relationship between $\chi_{eff}^{(2)}$ and the actual nonlinear susceptibility, $\chi_{ijk}^{(2)}$, is given by

$$\chi_{eff,ssp}^{(2)} = L_{yy}(\omega_{\mathrm{VSFG}}) L_{yy}(\omega_{\mathrm{vis}}) L_{zz}(\omega_{\mathrm{IR}}) \sin(\theta_{\mathrm{IR}}) \chi_{yyz}, \quad (2)$$

$$\chi_{eff,sps}^{(2)} = L_{yy}(\omega_{\mathrm{VSFG}}) L_{zz}(\omega_{\mathrm{vis}}) L_{yy}(\omega_{\mathrm{IR}}) \sin(\theta_{\mathrm{vis}}) \chi_{yzy}, \quad (3)$$

$$\chi_{eff,pss}^{(2)} = L_{zz}(\omega_{\mathrm{VSFG}}) L_{yy}(\omega_{\mathrm{vis}}) L_{yy}(\omega_{\mathrm{IR}}) \sin(\theta_{\mathrm{VSFG}}) \chi_{zyy}, \quad (4)$$

$$\begin{aligned} \chi_{eff,ppp}^{(2)} = & -L_{xx}(\omega_{\mathrm{VSFG}}) L_{xx}(\omega_{\mathrm{vis}}) L_{zz}(\omega_{\mathrm{IR}}) \cos(\theta_{\mathrm{VSFG}}) \cos(\theta_{\mathrm{vis}}) \sin(\theta_{\mathrm{IR}}) \chi_{xxz} \\ & -L_{xx}(\omega_{\mathrm{VSFG}}) L_{zz}(\omega_{\mathrm{vis}}) L_{xx}(\omega_{\mathrm{IR}}) \cos(\theta_{\mathrm{VSFG}}) \sin(\theta_{\mathrm{vis}}) \cos(\theta_{\mathrm{IR}}) \chi_{xzx} \\ & +L_{zz}(\omega_{\mathrm{VSFG}}) L_{xx}(\omega_{\mathrm{vis}}) L_{xx}(\omega_{\mathrm{IR}}) \sin(\theta_{\mathrm{VSFG}}) \cos(\theta_{\mathrm{vis}}) \cos(\theta_{\mathrm{IR}}) \chi_{zxx} \\ & +L_{zz}(\omega_{\mathrm{VSFG}}) L_{zz}(\omega_{\mathrm{vis}}) L_{zz}(\omega_{\mathrm{IR}}) \sin(\theta_{\mathrm{VSFG}}) \sin(\theta_{\mathrm{vis}}) \sin(\theta_{\mathrm{IR}}) \chi_{zzz}, \end{aligned} \quad (5)$$

where L_{ii} is the nonlinear Fresnel factor associated with ω_i, and θ_i is the input or output angle versus the surface normal for the associated beam (21, 29). By correcting for the nonlinear Fresnel

coefficients, it is possible to remove spectral contributions arising from experimental geometry, as recently demonstrated by Feng et al. (30) for the water spectra at the vapor/liquid interface for spectra originating from many research groups.

PS-SFG: phase-sensitive sum frequency generation

The resonant component of the Fresnel factor corrected second-order nonlinear susceptibility is related to the number density, N, of VSFG active oscillators and the molecular hyperpolarizability, β_v, through the orientationally averaged Euler angle transformation, $\langle \mu_{IJK:lmn} \rangle$, between the laboratory coordinates (IJK) and the molecular coordinates (lmn):

$$\chi^{(2)}_{IJK} = N \sum_{lmn} \langle \mu_{IJK:lmn} \rangle \beta_{lmn}. \tag{6}$$

The molecular hyperpolarizability term (Equation 7) is proportional to the Raman polarizability tensor for the transition moment $\langle g|\alpha_{lm}|v\rangle$ and the infrared transition moment $\langle v|\mu_n|g\rangle$. This gives rise to the VSFG selection rule that a vibrational mode must be both Raman and infrared active for VSFG to be allowed:

$$\beta_{lmn} = \frac{\langle g|\,\alpha_{lm}\,|v\rangle\,\langle v|\,\mu_n\,|g\rangle}{\omega_{\mathrm{IR}} - \omega_v + i\Gamma_v}, \tag{7}$$

$$\chi^{(2)}_{eff,v} \propto \frac{A_v}{\omega_{\mathrm{IR}} - \omega_v + i\Gamma_v}. \tag{8}$$

Generally, however, $\chi^{(2)}_{eff}$ is what is presented in the majority of published VSFG studies. Equation 8 reveals the Lorentzian lineshape character of the collected VSFG signal, where A_v is the SFG transition moment strength, ω_v is the frequency of the SFG active vibration, ω_{IR} is the frequency of the incident infrared laser beam, and Γ_v is the line width of the VSFG transition. It is clear from Equation 1 that during the collection of a conventional VSFG spectrum, the sign of the second-order nonlinear susceptibility is lost. This renders the direct collection of the orientation (phase) of the sum frequency transition impossible. Ji et al. (31) recently developed a generally applicable technique to directly measure the imaginary component (Equation 9) of the second-order nonlinear susceptibility, termed heterodyne-detected phase-sensitive sum frequency generation (PS-SFG), and it is being rapidly adopted by a few researchers within the surface spectroscopy field (32–35):

$$\mathrm{Im}\chi^{(2)}_v = -\sum_v \frac{A_v\Gamma_v}{(\omega_{\mathrm{IR}} - \omega_v)^2 + \Gamma_v^2}. \tag{9}$$

The vapor/neat water interface is perhaps the most simple, common, and important environmental interface. An understanding of this interface is especially vital from an atmospheric chemistry perspective as aqueous atmospheric aerosols are involved in a wide range of phenomena, from heterogeneous chemical reactions to global climate forcing (6, 36, 37). In 1993, Du et al. (11) completed the first study to utilize the VSFG method to investigate neat water structure at the vapor/water interface, showing the existence of three peaks at ~3,200 cm^{-1}, ~3,400 cm^{-1}, and ~3,700 cm^{-1} within the hydrogen-bonding continuum region between 3,000 and 3,800 cm^{-1}. The first two broad peaks at 3,200 cm^{-1} and 3,400 cm^{-1} are attributed to O-H stretching modes of hydrogen-bound water molecules similar to observations of bulk water with Raman and infrared spectroscopies (14), whereas the much narrower peak at 3,700 cm^{-1} is assigned to the dangling O-H stretch of water molecules that straddle the vapor/water interface. These dangling water molecules have one O-H bond pointing toward the vapor phase and the other O-H bond pointing toward the bulk liquid, where it is free to hydrogen bond with other water molecules (11). In the years following Du et al.'s study, many other researchers reproduced the VSFG

spectrum of the vapor/neat water interface, yet the exact origin of the VSFG spectral shape for the hydrogen-bonding continuum between 3,000 and 3,600 cm^{-1} remains controversial (16, 38–43).

Solute: a small, soluble, polyatomic molecular species

Lipid: molecule featuring a hydrophobic tail such as an alkyl chain with a hydrophilic head group such as a carboxylic acid

Beyond examining the water structure at the vapor/neat water interface, there is much interest in elucidating molecular behavior via VSFG at the vapor/water interface for a wide variety of chemical systems. With perspective toward understanding the role that tropospheric aqueous aerosols play in atmospheric chemistry, among other applications, VSFG has been applied to study the behavior that inorganic ions (25, 44–57), small molecular solutes (25, 58–69), and lipids (32, 35, 70–88) exhibit at the vapor/water interface as well as that of complex solutions that may involve multiple components such as multiple ion species and lipid monolayers spread on ion-containing subphases. At the vapor/water interface, it is critical to understand these three general classes of chemical systems, which increase in both size and surface preference from simple inorganic ions to solutes to lipids, as they influence the structure, growth, and reactivity of tropospheric aqueous aerosols.

In this review, we present recent insights gained through VSFG studies on the organization and reaction of atmospherically relevant chemical systems (ions, solutes, and lipids) to which the vapor/water interface plays host. Through the examination of both the response of water's hydrogen-bonding network at the vapor/liquid interface to the presence of these species and the vibrational modes of the chemical species themselves, elucidation of surface behavior is possible. In Section 2, the surface affinity of various inorganic salt-containing solutions is discussed, along with the effects these ionic species have on interfacial water structure. Included is a brief discussion of the recently developed PS-SFG technique and its application to the study of ions at the vapor/water interface. Section 3 discusses VSFG results for small molecular aqueous solutes. Here we highlight the surface organization and reaction of methanol at the vapor/aqueous interface. In Section 4, long-chain fatty acids are discussed, focusing on the surface organization, interaction with ionic species, and oxidation that may occur for these species at vapor/aqueous interfaces, as these are critical aspects in fat-coated aqueous aerosols. Section 5 briefly discusses future prospects of the application of VSFG to the study of environmental interfaces.

2. IONS

2.1. Water Structure as Influenced by Ions

The structure of inorganic ions at the vapor/water interface, as well as the relationship and effect these ions have on the structure of water's hydrogen-bonding network, is of special interest to the atmospheric chemistry community. The use of surface-specific vibrational spectroscopic techniques such as VSFG has been actively pursued by a number of groups to help elucidate long-standing questions on the surface hydrogen-bonding structure of water containing a wide variety of ions (14, 24, 25, 49, 50, 52, 89). Less work has examined the ion modes themselves owing to several factors, ranging from a lack of probable vibrational modes for atomic ions such as halides to the added experimental complexity in producing longer infrared wavelengths necessary to access molecular ionic vibrational modes. However, several recent studies have illustrated that this is possible for a variety of systems, and we discuss these results below (90–92). In this section we provide a brief synopsis of the major findings from work on vapor/ion-water interfaces using conventional VSFG completed by our lab and others on a number of inorganic salt-containing solutions as well as major unresolved questions remaining for these systems. Recent PS-SFG results on the hydrogen-bonding water structure at the vapor/aqueous salt solution interface are also highlighted.

Early VSFG work on aqueous inorganic salt solutions at the vapor/water interface primarily focused on quantifying differences observed between salt solutions and acidic solutions on the

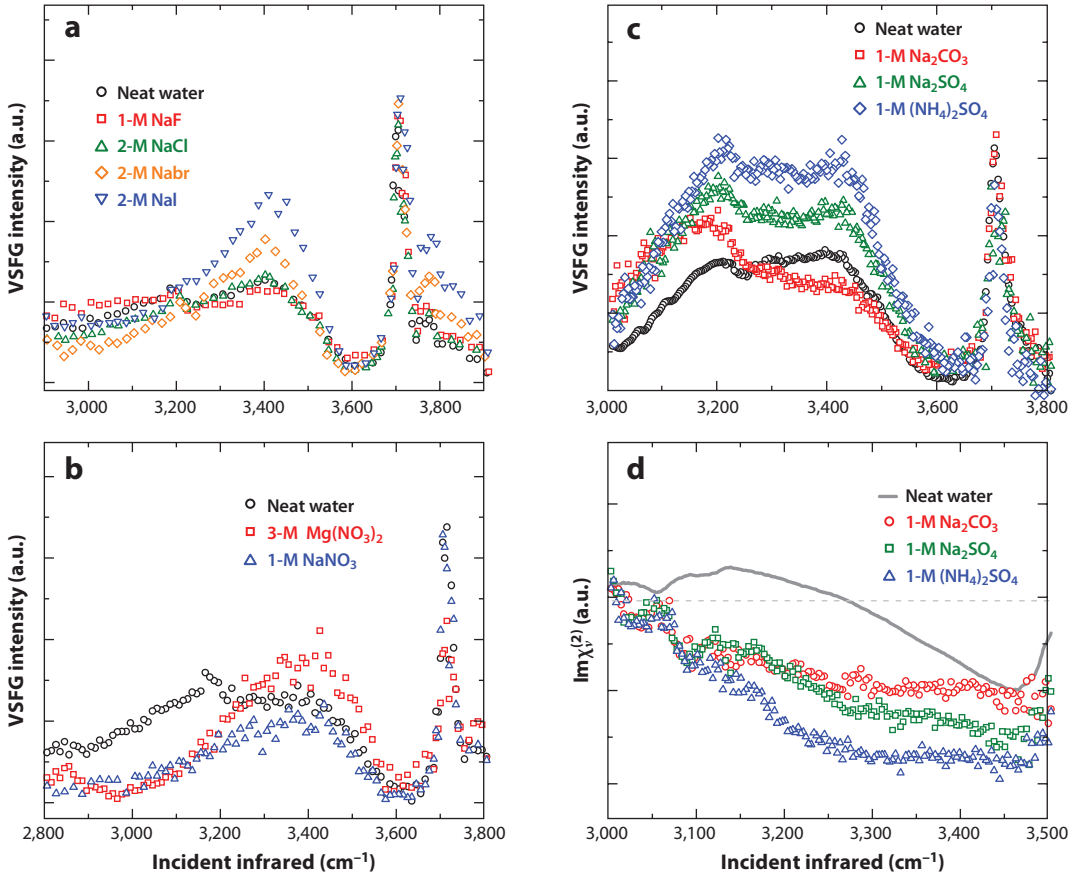

Figure 1

Conventional ssp polarized VSFG and $\mathrm{Im}\chi_v^{(2)}$ SFG spectra of neat water and aqueous solutions of (*a*) VSFG spectra of sodium halides, (*b*) VSFG spectra of 3-M $Mg(NO_3)_2$ and 1-M $NaNO_3$, (*c*) VSFG spectra of 1-M Na_2CO_3, 1-M Na_2SO_4, and 1-M $(NH_4)_2SO_4$, and (*d*) $\mathrm{Im}\chi_v^{(2)}$ SFG spectra of 1-M Na_2CO_3, 1-M Na_2SO_4, and 1-M $(NH_4)_2SO_4$. Figure adapted from References 46, 57, and 100.

hydrogen-bonding water structure at the vapor/solution interface. In 1997, Raduge et al. (45) and Baldelli et al. (55) were the first to report on the water structure at the vapor/solution interface for sulfuric-acid solutions. Following this work, Baldelli et al. (89) demonstrated in 1999 the influence of alkaline metal salts of sulfate and bisulfate on water structure. Later, Schnitzer et al. (56) extended the discussion to include a wider range of salts versus their acid analog. These experiments and others on a wider range of salts and acids have been repeated by several research groups, including ours (14, 49, 54).

In the past 10 years, the advancement of VSFG instrumentation has renewed interest in the effect that salts, especially halide salts (F^-, Cl^-, Br^-, and I^-) with mono- and divalent countercations (Na^+ and Mg^{2+}, Ca^{2+}, and Sr^{2+}), have on the water structure near the vapor/liquid interface, prompted by the work of Jungwirth & Tobias (93) predicting surface activity of some halides. The introduction of the halide salts, other than those containing fluoride, caused a slight decrease in the strong hydrogen-bonding region at 3,200 cm^{-1} and a significant increase in the weak hydrogen-bonding region at 3,400 cm^{-1} (**Figure 1*a***). These spectral changes increased with increasing polarizability of the anion ($Cl^- < Br^- < I^-$) and were interpreted as an indication

Local electric field: the electric field generated in the interface by the charge separation of cations and anions in ionic solutions

of the surface enrichment of solvated anions at the vapor/liquid interface, as an increase in the 3,400 cm^{-1} region intensity is also a signature for the halide's solvation shell water molecules (46). For fluoride-containing solutions, a slight decrease in both the 3,200 cm^{-1} and 3,400 cm^{-1} regions was observed by Raymond & Richmond (54). These observations, along with molecular dynamics simulation results, have been interpreted to represent the F^- ion being repelled from the interfacial region (54, 93). In contrast, for halide acid solutions (HCl, HBr, and HI), an enhancement of both the 3,200 cm^{-1} and 3,400 cm^{-1} regions is observed with VSFG. For the acids, the increase in the 3,400 cm^{-1} peak is again attributed to the enrichment of polarizable anions within the interfacial region, whereas the 3,200 cm^{-1} enhancement is attributed to hydronium ions residing within the interface convoluted with surface potential effects (47). Hydronium ions in halide acid systems have been suggested to both increase the interfacial depth and order water molecules within the interface (47, 50, 94). A comparison of the sodium halide salts to halide acid systems also reveals differences in the free O-H region, with a reduction in the free OH density for halide acids above 1 M (47, 51, 95).

The influence of molecular anions such as NO_3^-, SO_4^{2-}, and CO_3^{2-} on the hydrogen-bonding structure of water has also been the focus of many VSFG studies (14, 44, 48, 49, 53, 57, 96). An understanding of the VSFG results for polyatomic anion-containing solutions in the water hydrogen-bonding region proves more elusive than that for the halide salt solutions. For all nitrate-containing solutions (**Figure 1*b***), a severe depletion of the 3,200 cm^{-1} peak is observed, and for divalent cation–containing nitrate solutions, an enhancement of the 3,400 cm^{-1} region is observed, with the larger divalent cation–containing solutions exhibiting a greater enhancement of the 3,400 cm^{-1} region ($Sr^{2+} > Ca^{2+} > Mg^{2+}$). Solutions containing sulfate, with monovalent cations, however, feature a large enhancement for both the 3,200 cm^{-1} and 3,400 cm^{-1} peaks (**Figure 1*c***). (Divalent countercation solutions have not been measured.) Finally, sodium-carbonate solutions exhibit an enhancement of the 3,200 cm^{-1} peak and a depletion in the 3,400 cm^{-1} peak in VSFG spectra of the vapor/solution interface.

For nitrate systems, the significant depletion of the 3,200 cm^{-1} peak, and in some cases the enhancement of the 3,400 cm^{-1} peak, is taken as evidence that the nitrate ions reside within the vapor/water interface. The nitrate ion is thought to have comparable surface activity with that of the chloride ion such that even though nitrate exists within the interfacial region, no enrichment for the ion is observed (52, 57, 93, 96, 97). The magnitude for the decrease and increase of the 3,200 cm^{-1} and 3,400 cm^{-1} peaks, respectively, becomes more apparent for divalent cation–containing nitrate solutions as the size of the cation increases ($Mg^{2+} < Ca^{2+} < Sr^{2+}$). This has been attributed to the creation of complex concentration gradients by the larger divalent cations when paired with the nitrate ion such that the depth of the interfacial region increases (57); similar results have been found for the chloride ion when paired with divalent cations (95, 98). Recent PS-SFG studies are consistent with this picture (96).

For sodium-sulfate and ammonium-sulfate solutions (**Figure 1*c***), the enhancement for both the 3,200 cm^{-1} and 3,400 cm^{-1} regions has been attributed to the ordering of the interfacial water molecules by the local electric field that results from the sulfate dianion residing at the bottom of the interfacial region, with the cations residing some distance above the sulfate dianion (49, 53). Although this interpretation for VSFG results is somewhat speculative, it is in agreement with molecular dynamics simulations and PS-SFG studies for sulfate solutions, as shown in **Figure 1*d*** (discussed below) (53, 96, 99, 100). The larger spectral enhancement observed for ammonium-sulfate solutions compared with sodium-sulfate solutions is interpreted as a result of the ammonium ions' surface preference, which causes a greater separation between the ammonium and sulfate ions. This increased separation generates a local electric field with a greater magnitude within the interfacial region than what is generated with sodium-sulfate solutions and thus has a greater ordering effect on water molecules within the vapor/solution interface.

The sodium-carbonate results shown in **Figure 1*c*** are interpreted as follows: The enhancement of the 3,200 cm^{-1} peak is generally attributed to a convolution of an increase in the cooperative O-H stretching of tetrahedrally coordinated water molecules, the ordering effects of the ion-induced field, and strong ion-dipole interactions (44, 48, 49). The origin behind the decrease in the 3,400 cm^{-1} mode for sodium-carbonate solutions is unclear and is the subject of ongoing work.

The recent application of PS-SFG to the study of water organization at vapor/ion-water interfaces has confirmed many interpretations of these interfaces from conventional VSFG studies (48, 96, 100). Shown in **Figure 1*d*** are the $\mathrm{Im}\chi_v^{(2)}$ spectra obtained from PS-SFG for sodium-sulfate, ammonium-sulfate, and sodium-carbonate solutions. For both sulfate and carbonate, relative to the neat water surface, the change in sign from positive to negative from 3,000 to 3,200 cm^{-1} and the increased negative intensity of the 3,200–3,500 cm^{-1} region for the salt solutions compared to neat water reveal that both sulfate and carbonate have a strong orienting effect on the water OH transition moment, causing the water molecules to align with their OH transition moments pointing toward the bulk solution. This indicates that the dianions are residing near the bottom of the interfacial region, with the associated cations, ammonium and sodium, relatively near the surface. As a first estimate, the differences in spectral magnitude observed for the salt solutions in **Figure 1*d*** reveal the degree of separation between the cations and anions within the interface for the various salt solutions. Here the sulfate dianion resides deeper within the interface (well below the topmost surface) compared to carbonate, which results in a greater local electric field within the interface for sulfate solutions and exhibits a larger ordering effect on water molecules than is present in carbonate solutions. There is a similar explanation for the differences between ammonium-sulfate and sodium-sulfate solutions, as the ammonium ion is known to exhibit a greater surface preference than sodium, resulting in a larger charge separation of the ion pair within the interface (53).

2.2. Ion Interrogation

Beyond the examination of the effect ions have on the water structure at the vapor/water interface, it is possible to utilize VSFG to directly interrogate molecular ions at the vapor/water interface (90–92). These results often reveal surprising differences in ion behavior when compared to bulk studies of aqueous ions utilizing Raman and infrared spectroscopies (92, 101). Although little attention has been given to these types of studies because of added experimental complexity, we feel that several recent studies probing ion modes directly with VSFG at the vapor/water interface should be highlighted. Shown in **Figure 2** are spectra in the N-O vibrational region for the air/aqueous solution interface of 2.6 m and 3.3 m magnesium-nitrate solutions (here m is moles solute per kilogram solvent). It is also worth noting VSFG spectra published by Miyamae et al. (90) probing the S-O region at the vapor/liquid interface for a series of sulfuric-acid solutions from 0.01 x to 0.9 x mole fraction sulfuric acid, along with nitrate-ion spectra from nitric-acid solutions by Soule et al. (91).

The spectra shown in **Figure 2** feature two components that are both attributed to the symmetric stretching mode of the nitrate anion at the vapor/aqueous interface (92). As the concentration increases from 2.6 m to 3.3 m, the component at ~1,047 cm^{-1} increases dramatically. This is taken as evidence of ion-pair formation at the vapor/aqueous interface, in agreement with Raman experiments on the forced dehydration of supersaturated nitrate droplets (102). The work of Miyamae et al. (90) illustrates the surface activity of the sulfate dianion and speciation present as the concentration of H_2SO_4 increases from 0.01 x to 0.9 x mole fraction H_2SO_4. The little intensity for the dilute 0.01 x H_2SO_4 solution indicates that the sulfate dianion is repelled from the interface. However, as the concentration of H_2SO_4 increases to 0.39 x, approximately 98%

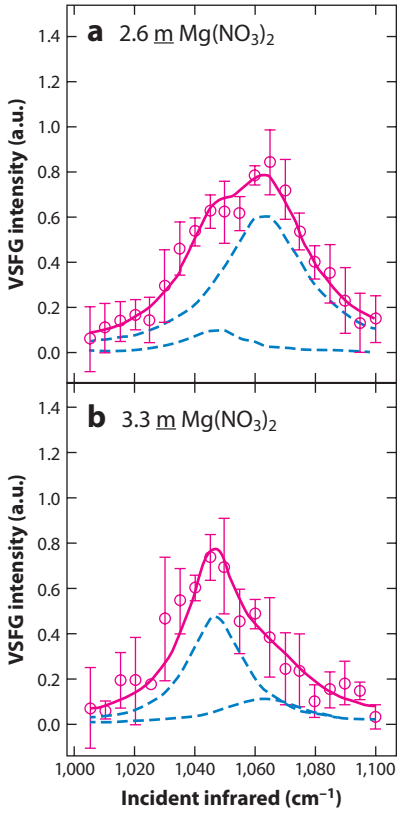

Figure 2

Conventional ssp polarized VSFG spectra of 2.6 m $Mg(NO_3)_2$ and 3.3 m $Mg(NO_3)_2$ solutions (where m is moles solute per kilogram solvent), demonstrating the symmetric stretch of the nitrate ion at the air-aqueous interface. Markers are data, the solid line is the fit, and the dashed lines are fit components. Figure reprinted with permission from Reference 92. Copyright 2009 American Chemical Society.

of the sulfate anions are protonated to form the bisulfate, HSO_4^-, anion, which can approach the interface. These studies demonstrate the sensitivity of VSFG to atmospherically relevant interfacial processes involving ions (90–92).

3. SOLUTES

3.1. Organization of Methanol

The surface preference and reaction of small soluble solutes at the air/vapor interface are also of great interest within the atmospheric chemistry community, and surface-specific optical spectroscopies such as VSFG and PS-SFG have been applied to study a wide range of these chemical systems (25, 58–69). Solutes generally differ in their behavior at vapor/water interfaces from what is observed for ions because of their larger molecular nature and the general, but not absolute, lack of a charge. Here we restrict the discussion to the simple alcohol methanol, CH_3OH, which has broad importance within tropospheric chemistry because it can be used as an alternative fuel and it is a common byproduct of plant biogenesis (6). Methanol is also known to impact both the

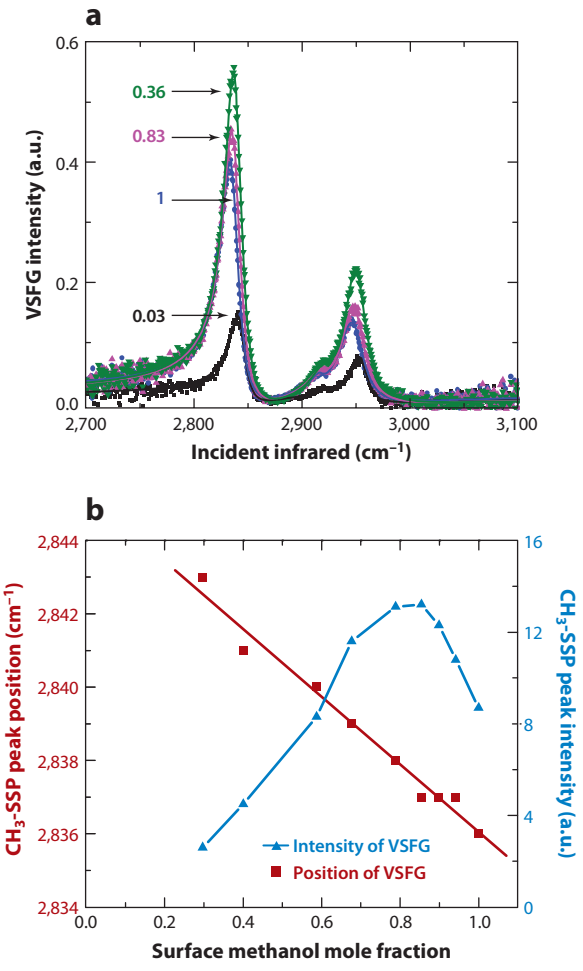

Figure 3

Conventional ssp polarized VSFG spectra, CH_3-ssp peak position, and intensity of aqueous methanol (CH_3OH) solutions. (*a*) VSFG spectra at different bulk methanol mole fractions. (*b*) CH_3-ssp peak position (*left y axis*) and intensity (*right y axis*) at different surface methanol mole fractions (with normalized surface number density). Figure adapted from Reference 67.

HO_x cycle and NO_y reactions and is involved in various heterogeneous chemical reactions that occur in methanol-containing aqueous aerosols (6, 67, 103–105). We first present the organization of methanol at the vapor/water interface with a perspective toward the evolving interpretation within the literature on its surface behavior. We then highlight the ability of VSFG to monitor surface reactions and the uptake of methanol for various vapor/aqueous interfaces (104). These studies underline the complex nature of reactions that can occur at interfacial regions and provide insight toward heterogeneous chemical reactions that may occur in tropospheric aerosols containing methanol.

Figure 3*a* shows the conventional VSFG spectra corresponding to a concentration series of binary water-methanol solutions from 0.03 x to 1.0 x mole fraction methanol at the vapor/aqueous interface. The spectra feature two peaks at ~2,840 cm^{-1} and ~2,950 cm^{-1} and a shoulder on the red side of the 2,950 cm^{-1} peak at ~2,920 cm^{-1}. The peak at 2,840 cm^{-1} is assigned to the

symmetric stretching mode of the methanol CH_3 moiety, whereas the other peak and shoulder are attributed to the Fermi resonances of the CH_3 symmetric stretch with the overtones of the CH_3 bending modes (58, 59, 62, 67, 68). By monitoring the position and intensity of the VSFG CH_3 symmetric stretch mode, one can infer a picture of methanol's surface behavior. As methanol molecules are surface active compared to water molecules in water-methanol binary mixtures, the bulk mole fraction of methanol does not accurately reflect the surface mole fraction. This has been accounted for in **Figure 3*b***, which shows the frequency and intensity shifts versus methanol's surface mole fraction (67). **Figure 3*b*** illustrates the red shift for the CH_3 symmetric stretch at the vapor/solution interface observed with VSFG by several researchers (58, 62, 67, 68). This red-shift trend is in agreement with Raman, infrared, and theoretical studies of bulk water–methanol mixtures and is generally accepted as indicating the increased hydrogen-bond-donor character methanol molecules exhibit as the water content decreases (67, 106, 107).

The most striking trend displayed by the spectra in **Figure 3*a*** is the decrease in the CH_3 symmetric stretch peak with the increase in methanol concentration above 0.8 x. This trend is not observed for bulk water–methanol studies utilizing Raman and infrared spectroscopies, but it has been observed for all VSFG studies at the vapor/solution interface (58, 62, 67, 68). Early studies by Wolfrum et al. (58) invoked VSFG's intensity dependence on net molecular orientation as well as number density (Equation 6) to explain the decrease in VSFG intensity with increased methanol concentrations. That is, as methanol concentration increases beyond 0.8 x, methanol at the vapor/solution interface becomes more disordered; subsequent VSFG studies by Huang & Wu (68) and Ma & Allen (67) and theoretical calculations by Paul & Chandra (108) confirmed this interpretation.

However, the polarization intensity ratio method (109) used in the above studies to probe methanol's reorientation with increased concentration yielded a large distribution of possible orientations. Recent VSFG studies utilizing the polarization null angle method to determine the molecular orientation for a variety of interfaces have shown the polarization null angle method to be more accurate than the widely used polarization intensity ratio method (21). In applying the polarization null angle methodology to the vapor/methanol-water binary mixture interface, Chen et al. (62) explored the notion that methanol undergoes reorientation with increased concentration at the vapor/solution interface and proposed that this is not the case. Their results indicate that methanol molecules are oriented with the CH_3 moiety approaching the surface normal directed toward the vapor phase for water-methanol binary mixtures and that this orientation does not significantly change with variation in methanol concentration. To explain the decrease in the VSFG signal observed with an increase in methanol concentration, Chen et al. proposed the presence of an antiparallel structure within the second layer from the surface of the interface, in line with VSFG findings for the vapor/solution interface of acetone-water mixtures (63, 64) and extended X-ray absorption fine-structure studies on the vapor/methanol interface (110). These conclusions have also been supported by the work of Sung et al. (69) for VSFG of alcohol-water binary mixtures and Monte Carlo calculations by Partay et al. (111).

3.2. Reactions with Sulfuric Acid

As indicated above for ions, VSFG provides the ability to monitor reactions that solute molecules undergo at surfaces beyond organization. Although many studies of this nature are present in the literature, we focus our discussion on methanol's uptake and reactions with sulfuric-acid solutions at the vapor/solution interface (103–105). Sulfuric acid is the end oxidation product of many sulfur-containing molecules produced in the atmospheric sulfur cycle; sulfur-containing

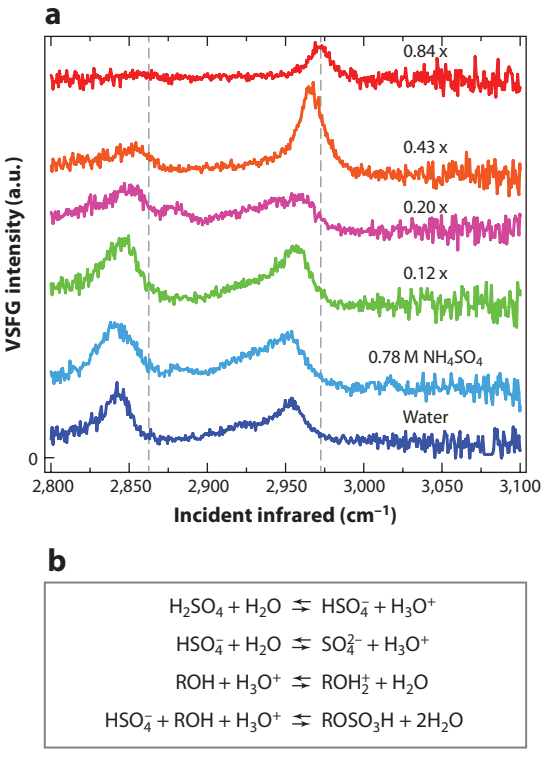

Figure 4

Conventional ssp polarized VSFG spectra and chemical reactions for the uptake of methanol at the surface of 0.12 x to 0.84 x mole fraction H_2SO_4 solutions. (*a*) VSFG spectra of methanol surface species at the solution vapor/liquid interfaces after 30 min of exposure to methanol vapor. (*b*) Relevant chemical reactions for the reaction of methanol with acidic media. Figure reprinted with permission from Reference 104. Copyright 2008 American Chemical Society.

molecules' strong affinity for water enables them to serve as cloud condensation nuclei and thus influence the albedo of the Earth (6, 36, 37).

Figure 4 illustrates VSFG spectra corresponding to the uptake and reaction of methanol vapor after 30 min of methanol exposure for water and a concentration series of sulfuric-acid solutions, along with the corresponding reaction sequence for the formation of methyl hydrogen sulfate (104). As the concentration of sulfuric acid increases (**Figure 4*a***), a blue shift and intensity change are apparent for the two peaks corresponding to the CH_3 symmetric stretch at ~2,840 cm^{-1} and the CH_3 Fermi resonance at ~2,954 cm^{-1} (compare with the methanol-water mixtures in **Figure 3*a***) until the peak at ~2,840 cm^{-1} has disappeared, for 0.84 x mole fraction sulfuric-acid solution, and the spectrum shows only one strong peak at ~2,972 cm^{-1}. The slight blue shift (~3 cm^{-1}) and intensity decrease observed for the 0.12 x and 0.20 x mole fraction sulfuric-acid-methanol solutions are consistent with the formation of protonated methanol, $CH_3OH_2^+$, within the interfacial region via the third reaction in **Figure 4*b*** (103). In the more concentrated sulfuric-acid solutions, the formation of methyl hydrogen sulfate, CH_3SO_4H, occurs within the vapor/solution interface via the fourth reaction pathway in **Figure 4*b***; this is apparent from the disappearance of the methanol CH_3 symmetric stretch peak at 2,840 cm^{-1} and the appearance of the strong peak at 2,972 cm^{-1} attributed to the CH_3 symmetric stretching mode of methyl hydrogen sulfate (103). These findings illustrate the ability of VSFG to monitor volatile organic

compounds such as methanol condensation onto and reaction with aqueous surfaces. Reactions such as the formation of methyl hydrogen sulfate highlight the transformation toward less volatile products, which can contribute to aerosol growth (104).

PA: palmitic acid

OA: oleic acid

SAM: self-assembled monolayer

4. LIPIDS

4.1. Palmitic Acid Organization and Ion Complexation

Organic coated aerosols have been shown to be ubiquitous in both marine and terrestrial environments. Palmitic acid (PA), $C_{16}H_{32}O_2$, and oleic acid (OA), $C_{18}H_{34}O_2$, are the most prevalent saturated and unsaturated fatty acid organic components found in fat-coated marine aqueous aerosols, respectively (112). Many studies have focused on elucidating the behavior of organic monolayers at the air/aqueous interface with fatty acid Langmuir film proxies, as this behavior has consequences for the growth of fat-coated aerosols and the reactions in which they take part (32, 70, 83, 85, 113–123). VSFG provides an excellent tool for explaining this behavior because of its inherent surface sensitivity. In this section, we review recent VSFG studies on the organization of PA monolayers at the air/aqueous interface as well as examine several reactions that PA monolayers may experience at the air/solution interface, such as ion complexation with ions contained within the solution subphase (74, 86, 88).

Figure 5*a* shows the spectrum of a PA self-assembled monolayer (SAM) on a neat water subphase in the C-H stretching region for a surface pressure of 10 mN m^{-1}. This spectrum features four signatures at 2,842 cm^{-1}, 2,874 cm^{-1}, 2,940 cm^{-1}, and 2,960 cm^{-1} that have been attributed to the methylene symmetric stretch, the methyl symmetric stretch, the methyl Fermi resonance, and the methyl asymmetric stretch, respectively (74, 88). The relative strength of the methyl symmetric stretch peak at 2,874 cm^{-1} compared with the methylene symmetric stretch at 2,842 cm^{-1} indicates the high degree of conformational order found in the PA SAM at a surface pressure of 10 mN m^{-1}. This is apparent when we consider that for a vibrational mode to be VSFG active, it must not feature an inversion center. The high methyl-to-methylene symmetric stretch ratio indicates that the PA molecules are highly aligned, inducing centrosymmetry between adjacent CH_2 moieties (124, 125); this feature is observed only for all-*trans* alkyl SAMs with an even number of methylene groups (88, 126).

When a PA monolayer is spread on aqueous subphases that contain ions (0.1- and 0.3-M $CaCl_2$; **Figure 5*b***), VSFG reveals slightly different behavior for the lipid SAM than what is observed for a neat water subphase. Here the overall spectral intensity in the C-H region observed for a PA monolayer is slightly greater than that observed for a PA monolayer on neat water; this suggests either that the PA molecules are more highly aligned when spread on an ionic subphase or that the monolayer packing has increased such that there is a greater number density of PA molecules within the VSFG probe spot. This can also be observed in the compression isotherm (**Figure 6*b***) for PA monolayers spread on neat water and $CaCl_2$-containing subphases. To quantitate these observations in the C-H region, Tang and colleagues (74, 88) investigated the COOH head group of PA to discover the effect ions have on the carboxyl and carboxylate symmetric stretching modes present at the vapor/solution interface. Shown in **Figure 5*c*,*d*** are spectra corresponding to the PA monolayer head group for PA SAMs spread on a pH-13 aqueous subphase, a 0.1-M $CaCl_2$ solution subphase, and a 0.3-M $CaCl_2$ subphase (**Figure 5*c***). The peak at ~1,410 cm^{-1} for the PA monolayer on the pH-13 subphase in **Figure 5*d*** has been assigned to the solvated COO^- symmetric stretch, indicating that the PA monolayer's head group is completely deprotonated at this pH, as is expected from attenuated total reflectance Fourier transform infrared studies by Gershevitz & Sukenik (113) on the pKa for carboxylate-terminated SAM. The spectra in **Figure 5*c***

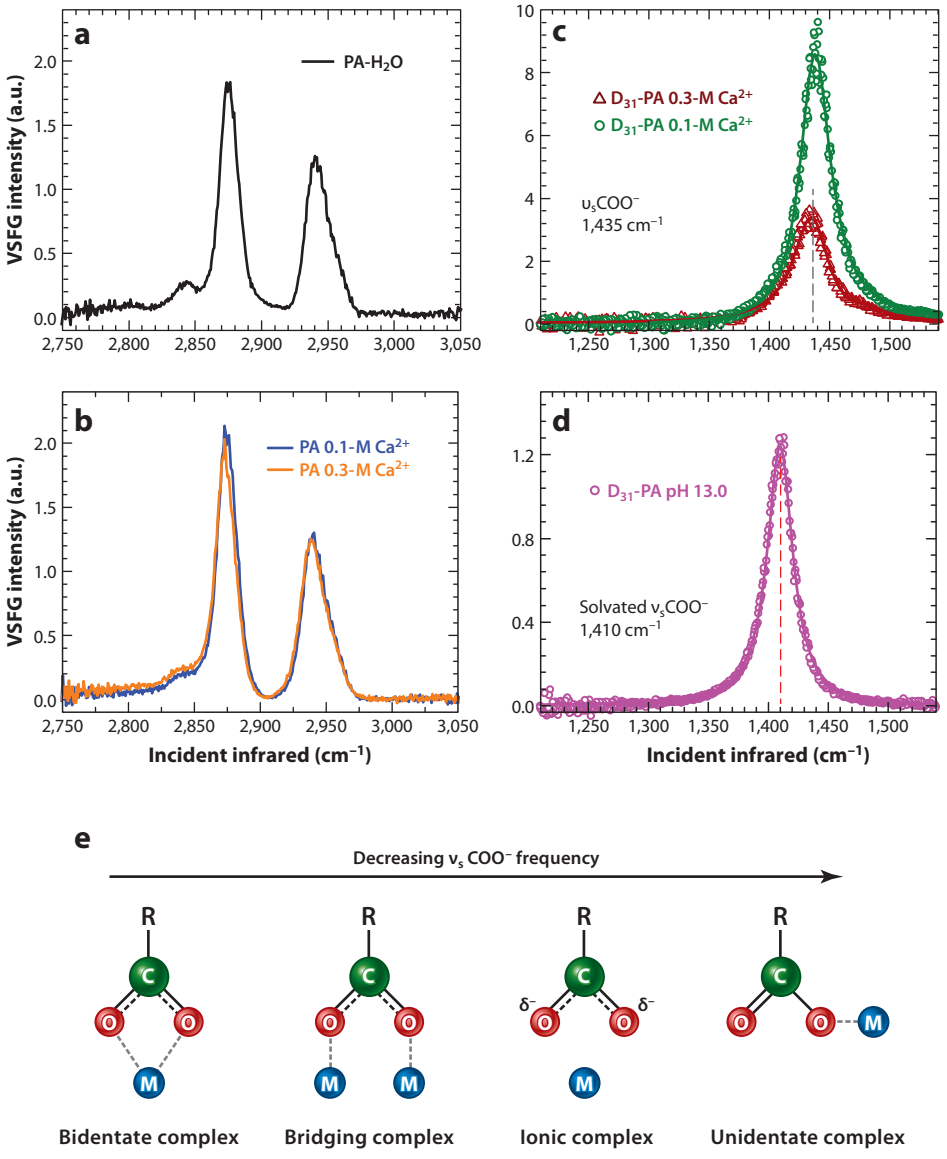

Figure 5

Conventional ssp polarized VSFG spectra of palmitic acid (PA) monolayers and schematic representation of ion complexation of the PA head group. (*a*) VSFG spectra in the C-H stretching region of PA monolayers on neat water at 10 mN m^{-1} and near neutral pH. (*b*) VSFG spectra in the C-H stretching region of a PA monolayer on 0.1- and 0.3-M $CaCl_2$ solutions. (*c*) VSFG spectra in the COO^- stretch region of D_{31}-PA monolayers on 0.1-and 0.3-M $CaCl_2$ solutions. (*d*) VSFG spectra in the COO^- stretch region of D_{31}-PA monolayers on water with pH 13.0. (*e*) Illustrations of four possible metal-carboxylate complexes in order of decreasing ν_s COO^- frequency. R represents an alkyl chain. Figure adapted from Reference 74.

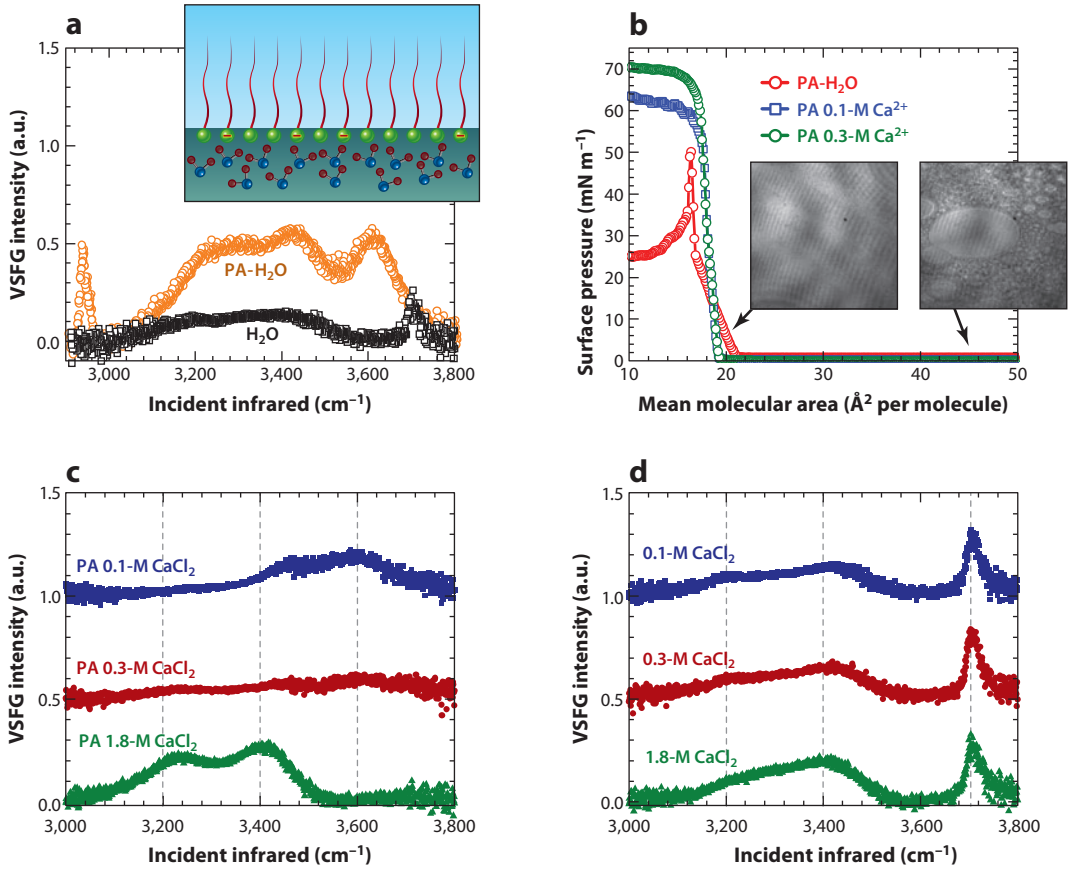

Figure 6

Conventional ssp polarized VSFG spectra and surface pressure–area isotherms (π-A) of a palmitic acid (PA) monolayer on aqueous surfaces at pH 6. (*a*) ssp VSFG spectrum of neat water and the PA monolayer on water at 23°C in the O-H stretching region. (*Inset*) A schematic of the PA monolayer organization on water. (*b*) Surface pressure–area isotherms (π-A) of the PA monolayer on an aqueous surface. (*Inset*) Brewster angle microscopy images corresponding to PA monolayers at the indicated surface pressures (*arrows*). (*c*) VSFG spectra in the O-H stretching region of neat water and $CaCl_2$ solutions (0.1, 0.3, and 1.8 M). (*d*) VSFG spectra in the O-H stretching region of PA monolayers on neat water and aqueous $CaCl_2$ solution (0.1, 0.3, and 1.8 M) subphases. Figure adapted from Reference 86.

corresponding to the PA SAM on $CaCl_2$ solutions show very different results; here the spectra are dominated by a strong peak at 1,435 cm^{-1}, and a slight shoulder at 1,475 cm^{-1} was also observed. These spectral features indicate the ion complexation that occurs between the aqueous cation and the ion-induced deprotonated COO^- head group with greater degrees of complexation, as illustrated in **Figure 5*e***, resulting in a larger blue shift in the COO^- frequency (127–129). The water structure near a PA SAM at the vapor/water and vapor/aqueous salt solution interfaces has also been examined with VSFG to elucidate the ultimate influence exerted by ion complexation and concomitant PA head-group deprotonation (86).

With regard to the water structure at the vapor/water interface for a variety of lipid SAMs, investigators have widely reported that the head-group charge and the packing ability of the SAM are the most dominant forces in influencing water organization near organic monolayers (32). **Figure *6a*** illustrates VSFG spectra in the O-H stretching region corresponding to neat water and a PA monolayer on a neat water subphase. The spectral enhancement of the O-H stretching peaks

for the PA monolayer results from the slight deprotonation of the PA head group at pH 6, which produces a surface charge. Surface charges have been shown to enhance water structure through charge-dipole interactions for a variety of systems at both the vapor/water and solid/water interfaces (31, 32, 35, 70, 87, 114, 130). These enhancements have also been widely attributed to $\chi^{(3)}$ effects, as first reported by Zhao et al. (114) for water near charged lipid monolayers. The inset of **Figure 6*a*** shows a physical representation of this. For PA monolayers spread on $CaCl_2$-containing subphases (**Figure 6*c***), the degree of enhancement observed for the peaks in the O-H region is less than that observed for PA on a neat water subphase, even for weakly concentrated (0.1-M) $CaCl_2$ solutions. This is further evidence of the ion complexation that occurs between the COO^- head group and Ca^{2+} ion in solution. Ion complexation effectively screens the surface charge induced by the deprotonated PA head group, as predicted by Gouy-Chapman theory (114, 130–133). The screening effect is seen to increase with Ca^{2+} concentration, as expected, until the water spectrum for a PA monolayer spread on a 1.8-M $CaCl_2$ subphase (**Figure 6*c***) resembles the water spectrum for a 1.8-M $CaCl_2$ solution without a PA monolayer at the vapor/solution interface (**Figure 6*d***), except for the disappearance of the peak at ~3,700 cm^{-1} (86). The disappearance of the 3,600 cm^{-1} peak in the spectra corresponding to the PA monolayer on the 1.8-M $CaCl_2$ subphase is the final confirmation that the head group of the associated PA molecules is completely deprotonated, as this mode has been attributed to the O-H mode of the protonated PA head group (32, 86).

Recently PS-SFG has been applied to the study of the water structure near charged and neutral Langmuir monolayers on neat water subphases (31–33, 35, 87, 123). These studies generally demonstrate the reorientation of water molecules causes the O-H transition dipole to point either toward or away from the charged monolayer, depending on the sign of the charge, although our recent work on zwitterions is an exception to this trend, as these act as negatively charged head groups (32). Nihonyanagi et al. (87) recently extended this method to study the water structure near charged lipid monolayers spread on NaCl-containing subphases and observed similar decreases in O-H peak intensity on the addition of salts, as is observed for a PA SAM spread on ion-containing subphases. Although Nihonyanagi et al. invoked electrolyte screening of a Gouy-Chapman electric double layer by the added salts and not an explicit ion-complexation argument, their results highlight the suitability of the PS-SFG technique to investigate complex lipid/ion/water systems.

These results demonstrate the intricate interactions that can occur for fat-coated marine aerosols between the surface organic film and the aqueous subphase. Interactions such as deprotonation have consequences for the growth and uptake of fat-coated aqueous aerosols as deprotonation can induce packing in the monolayer by reducing the charge repulsion of the head groups via ion complexation, with ions contained within the subphase such as Mg^{2+} and Ca^{2+} (74, 86, 88). Tightly packed monolayers are generally more resistant to water uptake because of the increased hydrophobicity of the outer layer, thus inhibiting further growth of the aerosol, although this idea has been challenged (105, 134, 135).

4.2. Oxidation of Oleic Acid Monolayers

Several researchers have recently applied VSFG to the study of the oxidation, generally by gaseous ozone (O_3), of tropospherically relevant organic films. Stokes and colleagues (136–138) used VSFG to monitor the reaction and reaction products of glass slides functionalized with tropospherically relevant organic moieties with ozone at the vapor/solid interface. Their results indicated reaction probabilities for a variety of organic moieties with ozone that are consistent with the molecular dynamics simulations of Vieceli et al. (139). At the vapor/liquid interface, more relevant to aqueous phase aerosols, Voss et al. (73) monitored the reaction for an OA monolayer on an aqueous

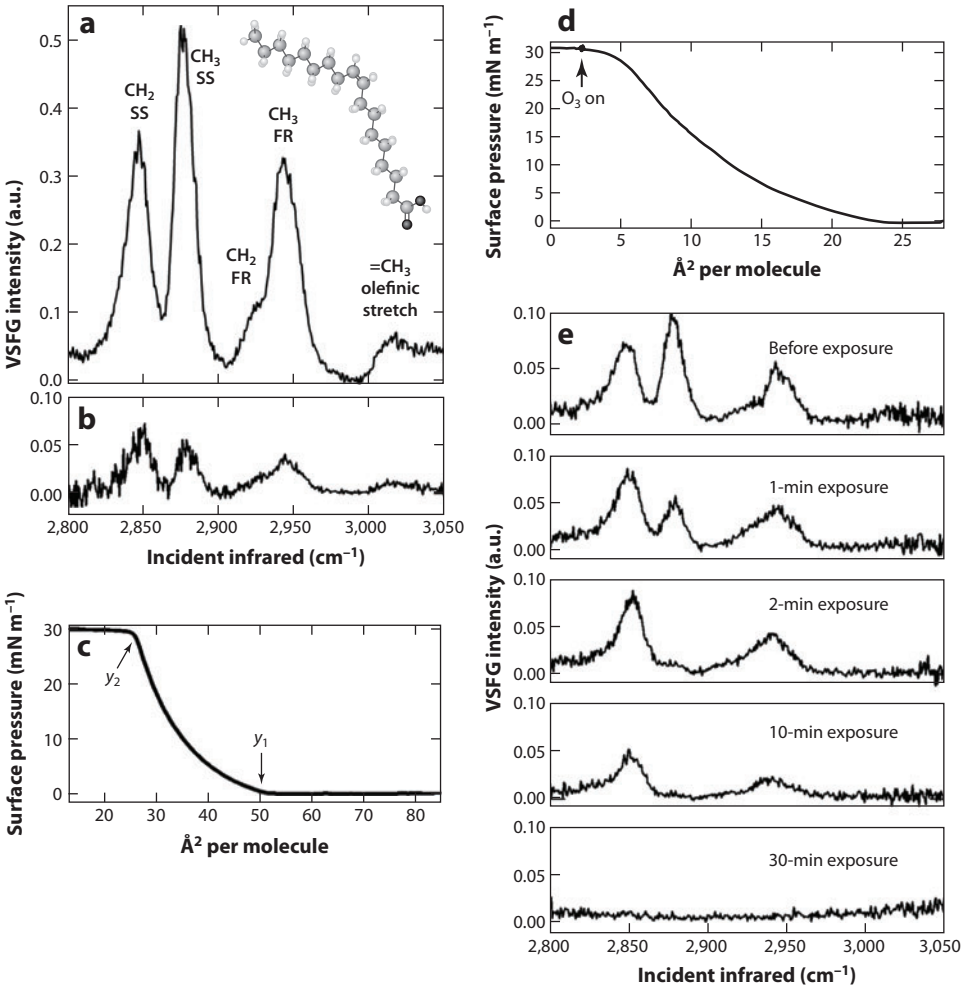

Figure 7

Conventional ssp polarized VSFG spectra and surface pressure–area isotherms (π-A) of oleic acid (OA) monolayers on neat water subphases. (*a*) VSFG spectrum of an OA monolayer on neat water at a surface pressure of ~12 mN m^{-1}. Abbreviations: FR, Fermi resonance; SS, symmetric stretch. (*Inset*) Molecular model of the OA molecule. (*b*) VSFG spectrum of an OA monolayer at a surface pressure of ~1 mN m^{-1}. (*c*) Langmuir compression isotherm with markers indicating the point of film collapse (y_2) and the point at which the VSFG spectrum of panel *b* (y_1) was acquired. (*d*) Langmuir isotherm during oxidation of oleic acid monolayer by ozone. (*e*) VSFG spectra corresponding to the oxidation of OA monolayers at the air/water interface with ozone after set exposure times. Figure reprinted with permission from Reference 73. Copyright 2007 American Geophysical Union.

subphase with ozone via VSFG. The oxidation of OA has been widely used as a proxy for the heterogeneous reaction of fat-coated aerosols with atmospheric oxidants because of its prevalence in atmospheric particulate matter (112, 115, 122, 140).

Here we focus the discussion on the oxidation for OA monolayers at the vapor/water interface by ozone in conjunction with the above discussion on the organization and reaction of atmospherically relevant fatty acid lipid monolayers. **Figure 7*a*** presents the VSFG spectrum of an OA

monolayer spread on a neat water subphase compressed to a surface pressure of ~12 mN m^{-1}, which corresponds to an average area per OA molecule in the film of 32 Å per molecule, slightly before the monolayer collapses at 28 Å per molecule indicated by point y_2 in **Figure 7*c***. There are five spectral features present in **Figure 7*a*** that are attributed to the CH_2 symmetric stretch (2,846 cm^{-1}), the CH_3 symmetric stretch (2,876 cm^{-1}), the CH_2 Fermi resonance (2,923 cm^{-1}), the CH_3 Fermi resonance (2,941 cm^{-1}), and the olefinic = CH stretch (3,014 cm^{-1}) (73). **Figure 7*b*** illustrates the VSFG spectrum for an OA monolayer slightly compressed to ~1 mN m^{-1}, indicated by point y_1 in **Figure 7*c***. Unlike for the PA monolayers discussed above, the CH_2 vibrational modes of the OA monolayer possess strong VSFG intensity owing to a lack of inversion for the CH_2 moieties, which results from the unsaturated nature of the OA molecule.

Spectra corresponding to the reaction of the OA film with ozone are shown in **Figure 7*e***, and the corresponding Langmuir isotherm during the oxidation is shown in **Figure 7*d***. Here an immediate drop in the CH_3 symmetric stretch peak is apparent after 1 min of exposure to ozone, and by 30 min of exposure, all VSFG signatures of the OA monolayer are gone. Through separate VSFG studies on the known reaction products of OA with ozone (140)—nonanal [$CH_3(CH_2)_7CHO$], nonanoic acid [$CH_3(CH_2)_7CO_2H$], azelaic acid [$HO_2C(CH_2)_7CO_2H$], and 9-oxononanoic acid [$OCH(CH_2)_7CO_2H$]—it was determined that the spectra shown in **Figure 7*e*** do not originate from reaction products at the vapor/water surface, which is consistent with the relatively high solubilities for these reaction products in water (141). To explain the observed spectral changes for the oxidation of OA, Voss et al. (73) compared the oxidation spectra (**Figure 7*e***) with the VSFG spectra observed for a slightly compressed (~1 mN m^{-1}), and thus disordered, OA monolayer at the vapor/water interface (**Figure 7*b***). The similarities between the spectra shown in **Figure 7*b*** and the spectra corresponding to the short ozone exposure times (1-min exposure) indicated that oxidation disordered the OA film. These results suggest that the oxidation of an organic film on an aqueous aerosol induces disorder within this film via the dissolution of the oxidation products into the aqueous subphase. This creates space for the unoxidized OA molecules to disperse owing to steric effects, analogous with observations for the slightly compressed OA monolayer (**Figure 7*b***) (73). This disorder may lead to the fragmentation of the aerosol or to heightened evaporation of the aqueous subphase; both these scenarios would lead to the formation of smaller fat-coated aerosols.

5. FUTURE PERSPECTIVES FOR VSFG OF ENVIRONMENTAL INTERFACES

Many recent advances in instrumentation and methodology have made the future of applying VSFG to the study of environmental interfacial processes a bright one. Perhaps the most exciting is the recent development of the PS-SFG technique (31), which enables the direct measurement of the transition dipole moment and provides insight into the organization of molecules. However, the application of this technique has been limited by the small number of research groups adopting it (31–33, 35), likely because of the complexity of the instrumentation and spectral processing. As an alternative, the utilization of the maximum entropy method has shown promise (18, 19, 34).

Recent advances have also been made for time-resolved VSFG measurements (142–144) as well as nonlinear optical spectroscopic measurements (145–148) from nonplanar interfaces such as colloidal suspensions. The ability to resolve dynamics at interfaces is a crucial step toward furthering the understanding of how molecules behave within the constrained interfacial region. Colloidal suspensions are ubiquitous in the environment and extremely important for the aqueous geochemistry of pollutant cycling (4).

SUMMARY POINTS

1. VSFG is a powerful tool for the investigation of environmental interfaces. Water molecules at the vapor/solution interface are shown to reorganize in the presence of ions. The size, charge, geometry, and polarizability of ions play a role in this reorganization, making PS-SFG direct measurements of the interfacial water structure important.
2. Solutes and lipids display very different behavior at the vapor/water interface than ions because of their increased surface preference. The orientation of these species at the surface can be determined through VSFG.
3. Reactions involving ions, solutes, and lipids in interfacial regimes are observable with VSFG. This is demonstrated by observing a series of various reactions for each class of systems: ion pairing between nitrate and the countercation at the vapor/solution interface, the reaction and uptake of methanol by sulfuric-acid solutions, and ion complexation and oxidation for various lipids spread on aqueous subphases.

DISCLOSURE STATEMENT

The authors are not aware of any affiliations, memberships, funding, or financial holdings that might be perceived as affecting the objectivity of this review.

ACKNOWLEDGMENTS

We acknowledge funding from the National Science Foundation (mainly MPS Chemistry, but also GEO Atmospheric Sciences), the Department of Energy Basic Energy Sciences – Geosciences, and the Camille and Henry Dreyfus Foundation for the Environmental Postdoctoral and the Teacher-Scholar Awards. In addition, we gratefully acknowledge previous contributions from former Allen group members. We also recognize the vast number of publications by others that we unfortunately were unable to reference owing to space limitations.

LITERATURE CITED

1. Chung SH, Andersen OS, Krishnamurthy V, eds. 2007. *Biological Membrane Ion Channnels: Dynamics, Structure, and Applications*. New York: Springer. 672 pp.
2. Berkowitz ML, Bostick DL, Pandit S. 2006. Aqueous solutions next to phospholipid membrane surfaces: insights from simulations. *Chem. Rev.* 106:1527–39
3. Lodish H, Berk A, Matsudaira P, Kaiser CA, Krieger M, et al. 2003. *Molecular Cell Biology*. New York: W.H. Freeman. 973 pp.
4. Langmuir D. 1997. *Aqueous Environmental Geochemistry*. Upper Saddle River, NJ: Prentice Hall. 600 pp.
5. Brown GE Jr, Henrich VE, Casey WH, Clark DL, Eggleston C, et al. 1999. Metal oxide surfaces and their interactions with aqueous solutions and microbial organisms. *Chem. Rev.* 99:77–174
6. Finlayson-Pitts BJ, Pitts JN Jr. 2000. *Chemistry of the Upper and Lower Atmosphere: Theory, Experiments and Applications*. San Diego: Academic. 969 pp.
7. **Franken PA, Ward JF. 1963. Optical harmonics and nonlinear phenomena. *Rev. Mod. Phys.* 35:23–39**
8. Shen YR. 1989. Surface properties probed by second-harmonic and sum-frequency generation. *Nature* 337:519–25
9. Shen YR. 1994. Surface spectroscopy by nonlinear optics. *Front. Laser Spectrosc.: Proc. Int. Sch. Phys. Enrico Fermi, 120th*, ed. TW Hansch, M Inguscio, pp. 139–65. Amsterdam: Elsevier Sci.

7. Demonstrates for the first time the experimental power of nonlinear optical phenomena.

10. Eisenthal KB. 1996. Liquid interfaces probed by second-harmonic and sum-frequency spectroscopy. *Chem. Rev.* 96:1343–60
11. Du Q, Superfine R, Freysz E, Shen YR. 1993. Vibrational spectroscopy of water at the vapor/water interface. *Phys. Rev. Lett.* 70:2313–16
12. Chen Z, Shen YR, Somorjai GA. 2002. Studies of polymer surfaces by sum frequency generation vibrational spectroscopy. *Annu. Rev. Phys. Chem.* 53:437–65
13. Schrodle S, Richmond GL. 2008. In situ non-linear spectroscopic approaches to understanding adsorption at mineral-water interfaces. *J. Phys. D Appl. Phys.* 41:033001
14. Gopalakrishnan S, Liu DF, Allen HC, Kuo M, Shultz MJ. 2006. Vibrational spectroscopic studies of aqueous interfaces: salts, acids, bases, and nanodrops. *Chem. Rev.* 106:1155–75
15. Morita A, Hynes JT. 2000. A theoretical analysis of the sum frequency generation spectrum of the water surface. *Chem. Phys.* 258:371–90
16. Auer BM, Skinner JL. 2009. Vibrational sum-frequency spectroscopy of the water liquid/vapor interface. *J. Phys. Chem. B* 113:4125–30
17. Noah-Vanhoucke J, Smith JD, Geissler PL. 2009. Statistical mechanics of sum frequency generation spectroscopy for the liquid-vapor interface of dilute aqueous salt solutions. *Chem. Phys. Lett.* 470:21–27
18. Sovago M, Vartiainen E, Bonn M. 2009. Determining absolute molecular orientation at interfaces: a phase retrieval approach for sum frequency generation spectroscopy. *J. Phys. Chem. C* 113:6100–6
19. Sovago M, Vartiainen E, Bonn M. 2010. Erratum: "Observation of buried water molecules in phospholipid membranes by surface sum-frequency generation spectroscopy (vol. 131, 161107, 2009)". *J. Chem. Phys.* 133:2
20. Jungwirth P, Tobias DJ. 2006. Specific ion effects at the air/water interface. *Chem. Rev.* 106:1259–81
21. Wang HF, Gan W, Lu R, Rao Y, Wu BH. 2005. Quantitative spectral and orientational analysis in surface sum frequency generation vibrational spectroscopy (SFG-VS). *Int. Rev. Phys. Chem.* 24:191–256
22. Geiger FM. 2009. Second harmonic generation, sum frequency generation, and $\chi^{(3)}$: dissecting environmental interfaces with a nonlinear optical Swiss Army knife. *Annu. Rev. Phys. Chem.* 60:61–83
23. Tyrode E, Rutland MW, Bain CD. 2008. Adsorption of CTAB on hydrophilic silica studied by linear and nonlinear optical spectroscopy. *J. Am. Chem. Soc.* 130:17434–45
24. Zhang YJ, Cremer PS. 2010. Chemistry of Hofmeister anions and osmolytes. *Annu. Rev. Phys. Chem.* 61:63–83
25. Shultz MJ, Schnitzer C, Simonelli D, Baldelli S. 2000. Sum frequency generation spectroscopy of the aqueous interface: ionic and soluble molecular solutions. *Int. Rev. Phys. Chem.* 19:123–53
26. Lambert AG, Davies PB. 2005. Implementing the theory of sum frequency generation vibrational spectroscopy: a tutorial review. *Appl. Spectrosc. Rev.* 40:103–45
27. Moad AJ, Simpson GJ. 2004. A unified treatment of selection rules and symmetry relations for sum-frequency and second harmonic spectroscopies. *J. Phys. Chem. B* 108:3548–62
28. Boyd RW. 1992. *Nonlinear Optics*. San Diego: Academic. 439 pp.
29. Miranda PB, Shen YR. 1999. Liquid interfaces: a study by sum-frequency vibrational spectroscopy. *J. Phys. Chem. B* 103:3292–307
30. Feng RR, Guo Y, Lu R, Velarde L, Wang HF. 2011. Consistency in the sum frequency generation intensity and phase vibrational spectra of the air/neat water interface. *J. Phys. Chem. A* 115:6015–27
31. Ji N, Ostroverkhov V, Chen CY, Shen YR. 2007. Phase-sensitive sum-frequency vibrational spectroscopy and its application to studies of interfacial alkyl chains. *J. Am. Chem. Soc.* 129:10056–57
32. Chen XK, Hua W, Huang ZS, Allen HC. 2010. Interfacial water structure associated with phospholipid membranes studied by phase-sensitive vibrational sum frequency generation spectroscopy. *J. Am. Chem. Soc.* 132:11336–42
33. Stiopkin IV, Jayathilake HD, Bordenyuk AN, Benderskii AV. 2008. Heterodyne-detected vibrational sum frequency generation spectroscopy. *J. Am. Chem. Soc.* 130:2271–75
34. de Beer AGF, Sampson JS, Hua W, Huang ZS, Chen XK, et al. 2011. Direct comparison of phase-sensitive vibrational sum frequency generation with maximum entropy method: case study of water. *J. Chem. Phys.* 135:224701

11. Observes for the first time the vapor/neat water interface with VSFG.

25. Summarizes early VSFG contributions to understanding molecular behavior at the vapor/solution interface for ionic solutions and solutes.

31. Demonstrates a generally applicable method for the experimental determination of the imaginary component of the second-order molecular susceptibility.

35. Nihonyanagi S, Yamaguchi S, Tahara T. 2009. Direct evidence for orientational flip-flop of water molecules at charged interfaces: a heterodyne-detected vibrational sum frequency generation study. *J. Chem. Phys.* 130:204704
36. Charlson RJ, Schwartz SE, Hales JM, Cess RD, Coakley JA, et al. 1992. Climate forcing by anthropogenic aerosols. *Science* 255:423–30
37. Schwartz SE. 1988. Are global cloud albedo and climate controlled by marine phytoplankton? *Nature* 336:441–45
38. Tian CS, Shen YR. 2009. Sum-frequency vibrational spectroscopic studies of water/vapor interfaces. *Chem. Phys. Lett.* 470:1–6
39. Sovago M, Campen RK, Bakker HJ, Bonn M. 2009. Hydrogen bonding strength of interfacial water determined with surface sum-frequency generation. *Chem. Phys. Lett.* 470:7–12
40. Fan YB, Chen X, Yang LJ, Cremer PS, Gao YQ. 2009. On the structure of water at the aqueous/air interface. *J. Phys. Chem. B* 113:11672–79
41. Smith JD, Cappa CD, Wilson KR, Cohen RC, Geissler PL, et al. 2005. Unified description of temperature-dependent hydrogen-bond rearrangement in liquid water. *Proc. Natl. Acad. Sci. USA* 102:14171–74
42. Raymond RA, Tarbuck TL, Brown MG, Richmond GL. 2003. Hydrogen-bonding interactions at the vapor/water interface investigated by vibrational sum-frequency spectroscopy of $HOD/H_2O/D_2O$ mixture and molecular dynamics simulations. *J. Phys. Chem. B* 107:546–56
43. Ishiyama T, Morita A. 2009. Analysis of anisotropic local field in sum frequency generation spectroscopy with the charge response kernel water model. *J. Chem. Phys.* 131:244714
44. Du H, Liu J, Ozdemir O, Nguyen AV, Miller JD. 2008. Molecular features of the air/carbonate solution interface. *J. Colloid Interface Sci.* 318:271–77
45. Raduge C, Pflumio V, Shen YR. 1997. Surface vibrational spectroscopy of sulfuric acid–water mixtures at the liquid-vapor interface. *Chem. Phys. Lett.* 274:140–44
46. Liu D, Ma G, Levering LM, Allen HC. 2004. Vibrational spectroscopy of aqueous sodium halide solutions and air-liquid interfaces: observation of increased interfacial depth. *J. Phys. Chem. B* 108:2252–60
47. Levering LM, Sierra-Hernandez MR, Allen HC. 2007. Observation of hydronium ions at the air–aqueous acid interface: vibrational spectroscopic studies of aqueous HCl, HBr, and HI. *J. Phys. Chem. C* 111:8814–26
48. Hua W, Chen X, Allen HC. 2011. Phase-sensitive sum frequency revealing accomodation of bicarbonate ions, and charge separation of sodium and carbonate ions within the air/water interface. *J. Phys. Chem. A* 115:6233–38
49. Tarbuck TL, Richmond GL. 2006. Adsorption and reaction of CO_2 and SO_2 at a water surface. *J. Am. Chem. Soc.* 128:3256–67
50. Tian CS, Ji N, Waychunas GA, Shen YR. 2008. Interfacial structures of acidic and basic aqueous solutions. *J. Am. Chem. Soc.* 130:13033–39
51. Mucha M, Frigato T, Levering LM, Allen HC, Tobias DJ, et al. 2005. Unified molecular picture of the surfaces of aqueous acid, base, and salt solutions. *J. Phys. Chem. B* 109:7617–23
52. Jungwirth P, Winter B. 2008. Ions at aqueous interfaces: from water surface to hydrated proteins. *Annu. Rev. Phys. Chem.* 59:343–66
53. Gopalakrishnan S, Jungwirth P, Tobias DJ, Allen HC. 2005. Air-liquid interfaces of aqueous solutions containing ammonium and sulfate: spectroscopic and molecular dynamics studies. *J. Phys. Chem. B* 109:8861–72
54. Raymond EA, Richmond GL. 2004. Probing the molecular structure and bonding of the surface of aqueous salt solutions. *J. Phys. Chem. B* 108:5051–59
55. Baldelli S, Schnitzer C, Shultz MJ, Campbell DJ. 1997. Sum frequency generation investigation of water at the surface of H_2O/H_2SO_4 binary systems. *J. Phys. Chem. B* 101:10435–41
56. Schnitzer C, Baldelli S, Shultz MJ. 2000. Sum frequency generation of water on NaCl, $NaNO_3$, $KHSO_4$, HCl, HNO_3, and H_2SO_4 aqueous solutions. *J. Phys. Chem. B* 104:585–90
57. Xu M, Spinney R, Allen HC. 2009. Water structure at the air-aqueous interface of divalent cation and nitrate solutions. *J. Phys. Chem. B* 113:4102–10

46. Observes the increase in interfacial depth upon salt addition at the vapor/solution interface via VSFG.

47. Observes the presence of hydronium ions in the vapor/solution interface for HCl, HBr, and HI solutions.

58. Wolfrum K, Graener H, Laubereau A. 1993. Sum-frequency vibrational spectroscopy at the liquid-air interface of methanol: water solutions. *Chem. Phys. Lett.* 213:41–46
59. Superfine R, Huang JY, Shen YR. 1991. Nonlinear optical studies of the pure liquid/vapor interface: vibrational spectra and polar ordering. *Phys. Rev. Lett.* 66:1066–69
60. Allen HC, Raymond EA, Richmond GL. 2000. Nonlinear vibrational sum frequency generation spectroscopy of atmospherically relevant molecules at aqueous solution surfaces. *Curr. Opin. Colloid Interface Sci.* 5:74–80
61. Allen HC, Raymond EA, Richmond GL. 2001. Surface structural studies of methanesulfonic acid at air/aqueous solution interfaces using vibrational sum frequency spectroscopy. *J. Phys. Chem. A* 105:1649–55
62. Chen H, Gan W, Lu R, Guo Y, Wang H-F. 2005. Determination of structure and energetics for Gibbs surface adsorption layers of binary liquid mixture 2. Methanol + water. *J. Phys. Chem. B* 109:8064–75
63. Chen H, Gan W, Wu B-H, Wu D, Guo Y, et al. 2005. Determination of structure and energetics for Gibbs surface adsorption layers of binary liquid mixture 1. Acetone + water. *J. Phys. Chem. B* 109:8053–63
64. Chen H, Gan W, Wu B-H, Wu D, Zhang Z, et al. 2005. Determination of the two methyl group orientations at vapor/acetone interface with polarization null angle method in SFG vibrational spectroscopy. *Chem. Phys. Lett.* 408:284–89
65. Chen XK, Allen HC. 2010. Water structure at aqueous solution surfaces of atmospherically relevant dimethyl sulfoxide and methanesulfonic acid revealed by phase-sensitive sum frequency spectroscopy. *J. Phys. Chem. B* 114:14983–88
66. Chen XK, Minofar B, Jungwirth P, Allen HC. 2010. Interfacial molecular organization at aqueous solution surfaces of atmospherically relevant dimethyl sulfoxide and methanesulfonic acid using sum frequency spectroscopy and molecular dynamics simulation. *J. Phys. Chem. B* 114:15546–53
67. Ma G, Allen HC. 2003. Surface studies of aqueous methanol solutions by vibrational broad bandwidth sum frequency generation spectroscopy. *J. Phys. Chem. B* 107:6343–49
68. Huang JY, Wu MH. 1994. Nonlinear optical studies of binary mixtures of hydrogen-bonded liquids. *Phys. Rev. E* 50:3737–46
69. Sung JH, Park K, Kim D. 2005. Surfaces of alcohol-water mixtures studied by sum-frequency generation vibrational spectroscopy. *J. Phys. Chem. B* 109:18507–14
70. Miranda PB, Du Q, Shen YR. 1998. Interaction of water with a fatty acid Langmuir film. *Chem. Phys. Lett.* 286:1–8
71. Ma G, Allen HC. 2007. Condensing effect of palmitic acid on DPPC in mixed Langmuir monolayers. *Langmuir* 23:589–97
72. Ma G, Chen XK, Allen HC. 2007. Dangling OD confined in a Langmuir monolayer. *J. Am. Chem. Soc.* 129:14053–57
73. Voss LF, Bazerbashi MF, Beekman CP, Hadad CM, Allen HC. 2007. Oxidation of oleic acid at air/liquid interfaces. *J. Geophys. Res. Atmos.* 112:D06209
74. Tang CY, Huang ZS, Allen HC. 2010. Binding of Mg^{2+} and Ca^{2+} to palmitic acid and deprotonation of the COOH headgroup studied by vibrational sum frequency generation spectroscopy. *J. Phys. Chem. B* 114:17068–76
75. Hunt JH, Guyot-Sionnest P, Shen YR. 1987. Observation of C-H stretch vibrations of monolayers of molecules using optical sum-frequency generation. *Chem. Phys. Lett.* 133:189–92
76. Conboy JC, Messmer MC, Richmond GL. 1997. Dependence of alkyl chain conformation of simple ionic surfactants on head group functionality as studied by vibrational sum-frequency spectroscopy. *J. Phys. Chem. B* 101:6724–33
77. Muller M, Schins JM, Roke S, Bonn M. 2003. Phase transitions in a lipid monolayer observed with vibrational sum-frequency generation. *Proc. SPIE* 4964:90–97
78. Ma G, Allen HC. 2006. DPPC Langmuir monolayer at the air-water interface: probing the tail and head groups by vibrational sum frequency generation spectroscopy. *Langmuir* 22:5341–49
79. Harper KL, Allen HC. 2007. Competition between DPPC and SDS at the air-aqueous interface. *Langmuir* 23:8925–31
80. Gragson DE, McCarty BM, Richmond GL. 1996. Surfactant/water interactions at the air/water interface probed by vibrational sum frequency generation. *J. Phys. Chem.* 100:14272–75

81. Conboy JC, Messmer MC, Walker RA, Richmond GL. 1997. An investigation of surfactant behavior at the liquid/liquid interface with sum-frequency vibrational spectroscopy. *Prog. Colloid Polym. Sci.* 103:10–20
82. Watry MR, Tarbuck TL, Richmond GL. 2003. Vibrational sum-frequency studies of a series of phospholipid monolayers and the associated water structure at the vapor/water interface. *J. Phys. Chem. B* 107:512–18
83. Hore DK, Beaman DK, Richmond GL. 2005. Surfactant headgroup orientation at the air/water interface. *J. Am. Chem. Soc.* 127:9356–57
84. Nickolov ZS, Britt DW, Miller JD. 2006. Sum-frequency spectroscopy analysis of two-component Langmuir monolayers and the associated interfacial water structure. *J. Phys. Chem. B* 110:15506–13
85. Wang HF, Zhao XL, Eisenthal KB. 2000. Effects of monolayer density and bulk ionic strength on acid-base equilibria at the air/water interface. *J. Phys. Chem. B* 104:8855–61
86. Tang CY, Huang ZS, Allen HC. 2010. Interfacial water structure and effects of Mg^{2+} and Ca^{2+} binding to the COOH headgroup of a palmitic acid monolayer studied by sum frequency spectroscopy. *J. Phys. Chem. B* 115:34–40
87. Nihonyanagi S, Yamaguchi S, Tahara T. 2010. Water hydrogen bond structure near highly charged interfaces is not like ice. *J. Am. Chem. Soc.* 132:6867–69
88. Tang C, Allen HC. 2009. Ionic binding of Na^+ versus K^+ to the carboxylic acid headgroup of palmitic acid monolayers studied by vibrational sum frequency generation spectroscopy. *J. Phys. Chem. A* 113:7383–93
89. Baldelli S, Schnitzer C, Campbell DJ, Shultz MJ. 1999. Effect of H_2SO_4 and alkali metal SO_4^{2-}/HSO_4^- salt solutions on surface water molecules using sum frequency generation. *J. Phys. Chem. B* 103:2789–95
90. Miyamae T, Morita A, Ouchi Y. 2008. First acid dissociation at an aqueous H_2SO_4 interface with sum frequency generation spectroscopy. *Phys. Chem. Chem. Phys.* 10:2010–13
91. Soule MCK, Blower PG, Richmond GL. 2007. Nonlinear vibrational spectroscopic studies of the adsorption and speciation of nitric acid at the vapor/acid solution interface. *J. Phys. Chem. A* 111:3349–57
92. Xu M, Tang CY, Jubb AM, Chen XK, Allen HC. 2009. Nitrate anions and ion pairing at the air-aqueous interface. *J. Phys. Chem. C* 113:2082–87
93. Jungwirth P, Tobias DJ. 2001. Molecular structure of salt solutions: a new view of the interface with implications for heterogeneous atmospheric chemistry. *J. Phys. Chem. B* 105:10468–72
94. Petersen PB, Saykally RJ. 2005. Evidence for an enhanced hydronium concentration at the liquid water surface. *J. Phys. Chem. B* 109:7976–80
95. Allen HC, Casillas-Ituarte NN, Sierra-Hernandez MR, Chen XK, Tang CY. 2009. Shedding light on water structure at air-aqueous interfaces: ions, lipids, and hydration. *Phys. Chem. Chem. Phys* 11:5538–49
96. Tian CS, Byrnes SJ, Han HL, Shen YR. 2011. Surface propensities of atmospherically-relevant ions in salt solutions revealed by phase-sensitive sum frequency vibrational spectroscopy. *J. Phys. Chem. Lett.* 2:1946–49
97. Pegram LM, Record MT. 2006. Partitioning of atmospherically relevant ions between bulk water and the water/vapor interface. *Proc. Natl. Acad. Sci. USA* 103:14278–81
98. Casillas-Ituarte NN, Callahan KM, Tang CY, Chen XK, Roeselova M, et al. 2010. Surface organization of aqueous $MgCl_2$ and application to atmospheric marine aerosol chemistry. *Proc. Natl. Acad. Sci. USA* 107:6616–21
99. Jungwirth P, Curtis JE, Tobias DJ. 2003. Polarizability and aqueous solvation of the sulfate dianion. *Chem. Phys. Lett.* 367:704–10
100. Hua W, Jubb AM, Allen HC. 2011. Electric field reversal of Na_2SO_4, $(NH_4)_2SO_4$, and Na_2CO_3 relative to $CaCl_2$ and NaCl at the air/aqueous interface revealed by phase-sensitive sum frequency. *J. Phys. Chem. Lett.* 2:2515–20
101. Xu M, Larentzos JP, Roshdy M, Criscenti LJ, Allen HC. 2008. Aqueous divalent metal-nitrate interactions: hydration versus ion pairing. *Phys. Chem. Chem. Phys.* 10:4793–801
102. Li XH, Zhao LJ, Dong JL, Xiao HS, Zhang YH. 2008. Confocal Raman studies of $Mg(NO_3)_2$ aerosol particles deposited on a quartz substrate: supersaturated structures and complicated phase transitions. *J. Phys. Chem. B* 112:5032–38

86. Illustrates the strong binding between palmitic acid monolayer head groups and divalent cations contained within the aqueous subphase.

103. Van Loon LL, Allen HC. 2004. Methanol reaction with sulfuric acid: a vibrational spectroscopic study. *J. Phys. Chem. B* 108:17666–74
104. Van Loon LL, Allen HC. 2008. Uptake and surface reaction of methanol by sulfuric acid solutions investigated by vibrational sum frequency generation and Raman spectroscopies. *J. Phys. Chem. A* 112:7873–80
105. Van Loon LL, Minor RN, Allen HC. 2007. Structure of butanol and hexanol at aqueous, ammonium bisulfate, and sulfuric acid solution surfaces investigated by vibrational sum frequency generation spectroscopy. *J. Phys. Chem. A* 111:7338–46
106. Gruenloh CJ, Florio GM, Carney JR, Hagemeister FC, Zwier TS. 1999. C-H stretch modes as a probe of H-bonding in methanol-containing clusters. *J. Phys. Chem. A* 103:496–502
107. Dixit S, Poon WCK, Crain J. 2000. Hydration of methanol in aqueous solutions: a Raman spectroscopic study. *J. Phys. Condens. Matter* 12:L323–28
108. Paul S, Chandra A. 2005. Hydrogen bond properties and dynamics of liquid-vapor interfaces of aqueous methanol solutions. *J. Chem. Theory Comput.* 1:1221–31
109. Zhuang X, Miranda PB, Kim D, Shen YR. 1999. Mapping molecular orientation and conformation at interfaces by surface nonlinear optics. *Phys. Rev. B* 59:12632–40
110. Wilson KR, Schaller RD, Co DT, Saykally RJ, Rude BS, et al. 2002. Surface relaxation in liquid water and methanol studied by X-ray absorption spectroscopy. *J. Chem. Phys.* 117:7738–44
111. Partay L, Jedlovszky P, Vincze A, Horvai G. 2005. Structure of the liquid-vapor interface of water-methanol mixtures as seen from Monte Carlo simulations. *J. Phys. Chem. B* 109:20493–503
112. Tervahattu H, Juhanoja J, Kupiainen K. 2002. Identification of an organic coating on marine aerosol particles by TOF-SIMS. *J. Geophys. Res. Atmos.* 107:4319
113. Gershevitz O, Sukenik CN. 2004. In situ FTIR-ATR analysis and titration of carboxylic acid-terminated SAMs. *J. Am. Chem. Soc.* 126:482–83
114. Zhao XL, Ong SW, Eisenthal KB. 1993. Polarization of water molecules at a charged interface: second harmonic studies of charged monolayers at the air/water interface. *Chem. Phys. Lett.* 202:513–20
115. Ellison GB, Tuck AF, Vaida V. 1999. Atmospheric processing of organic aerosols. *J. Geophys. Res. Atmos.* 104:11633–41
116. Kaganer VM, Mohwald H, Dutta P. 1999. Structure and phase transitions in Langmuir monolayers. *Rev. Mod. Phys.* 71:779–819
117. Gurau MC, Castellana ET, Albertorio F, Kataoka S, Lim S-M, et al. 2003. Thermodynamics of phase transitions in Langmuir monolayers observed by vibrational sum frequency spectroscopy. *J. Am. Chem. Soc.* 125:11166–67
118. Gurau MC, Kim G, Lim SM, Albertorio F, Fleisher HC, et al. 2003. Organization of water layers at hydrophilic interfaces. *ChemPhysChem* 4:1231–33
119. Johnson CM, Tyrode E. 2005. Study of the adsorption of sodium dodecyl sulfate (SDS) at the air/water interface: targeting the sulfate headgroup using vibrational sum frequency spectroscopy. *Phys. Chem. Chem. Phys.* 7:2635–40
120. Tyrode E, Niga P, Johnson M, Rutland MW. 2010. Molecular structure upon compression and stability toward oxidation of Langmuir films of unsaturated fatty acids: a vibrational sum frequency spectroscopy study. *Langmuir* 26:14024–31
121. Tian CS, Shen YR. 2009. Structure and charging of hydrophobic material/water interfaces studied by phase-sensitive sum-frequency vibrational spectroscopy. *Proc. Natl. Acad. Sci. USA* 106:15148–53
122. Zahardis J, Petrucci GA. 2007. The oleic acid–ozone heterogeneous reaction system: products, kinetics, secondary chemistry, and atmospheric implications of a model system—a review. *Atmos. Chem. Phys.* 7:1237–74
123. Mondal JA, Nihonyanagi S, Yamaguchi S, Tahara T. 2010. Structure and orientation of water at charged lipid monolayer/water interfaces probed by heterodyne-detected vibrational sum frequency generation spectroscopy. *J. Am. Chem. Soc.* 132:10656–57
124. Ma G, Allen HC. 2006. New insights into lung surfactant monolayers using vibrational sum frequency generation spectroscopy. *Photochem. Photobiol.* 82:1517–29
125. Can SZ, Mago DD, Walker RA. 2006. Structure and organization of hexadecanol isomers adsorbed to the air/water interface. *Langmuir* 22:8043–49

104. Highlights the ability of VSFG to monitor the reaction and uptake for methanol at acidic solution surfaces.

126. Miranda PB, Pflumio V, Saijo H, Shen YR. 1998. Chain-chain interaction between surfactant monolayers and alkanes or alcohols at solid/liquid interfaces. *J. Am. Chem. Soc.* 120:12092–99
127. Nakamoto K. 1957. Infrared spectra of metallic complexes IV. Comparison of the infrared spectra of unidentate and bidentate metallic complexes. *J. Am. Chem. Soc.* 79:4904–8
128. Nakamoto K. 1986. *Infrared and Raman Spectra of Inorganic and Coordination Compounds*. New York: Wiley
129. Tackett JE. 1989. FT-IR characterization of metal acetates in aqueous solution. *Appl. Spectrosc.* 43:483–89
130. Ong S, Zhao X, Eisenthal KB. 1992. Polarization of water molecules at a charged interface: second harmonic studies of the silica/water interface. *Chem. Phys. Lett.* 191:327–35
131. Hopkins AJ, Schrodle S, Richmond GL. 2010. Specific ion effects of salt solutions at the CaF_2/water interface. *Langmuir* 26:10784–90
132. Adamson AW, Gast AP. 1997. *Physical Chemistry of Surfaces*. New York: Wiley. 784 pp.
133. Gragson DE, McCarty BM, Richmond GL. 1997. Ordering of interfacial water molecules at the charged air/water interface observed by vibrational sum frequency generation. *J. Am. Chem. Soc.* 119:6144–52
134. Lawrence JR, Glass SV, Nathanson GM. 2005. Evaporation of water through butanol films at the surface of supercooled sulfuric acid. *J. Phys. Chem. A* 109:7449–57
135. Lawrence JR, Glass SV, Park SC, Nathanson GM. 2005. Surfactant control of gas uptake: effect of butanol films on HCl and HBr entry into supercooled sulfuric acid. *J. Phys. Chem. A* 109:7458–65
136. Voges AB, Stokes GY, Gibbs-Davis JM, Lettan RB II, Bertin PA, et al. 2007. Insights into heterogeneous atmospheric oxidation chemistry: development of a tailor-made synthetic model for studying tropospheric surface chemistry. *J. Phys. Chem. C* 111:1567–78
137. Stokes GY, Buchbinder AM, Gibbs-Davis JM, Scheidt KA, Geiger FM. 2008. Heterogeneous ozone oxidation reactions of 1-pentene, cyclopentene, cyclohexene, and a menthenol derivative studied by sum frequency generation. *J. Phys. Chem. A* 112:11688–98
138. Stokes GY, Buchbinder AM, Gibbs-Davis JM, Scheidt KA, Geiger FM. 2009. Chemically diverse environmental interfaces and their reactions with ozone studied by sum frequency generation. *Vib. Spectrosc.* 50:86–98
139. Vieceli J, Ma OL, Tobias DJ. 2004. Uptake and collision dynamics of gas phase ozone at unsaturated organic interfaces. *J. Phys. Chem. A* 108:5806–14
140. Moise T, Rudich Y. 2002. Reactive uptake of ozone by aerosol-associated unsaturated fatty acids: kinetics, mechanism, and products. *J. Phys. Chem. A* 106:6469–76
141. Yalkowsky SH, He Y. 2003. *Handbook of Aqueous Solubility Data*. Boca Raton, FL: CRC. 1496 pp.
142. Rao Y, Turro NJ, Eisenthal KB. 2010. Solvation dynamics at the air/water interface with time-resolved sum-frequency generation. *J. Phys. Chem. C* 114:17703–8
143. Nienhuys HK, Bonn M. 2009. Measuring molecular reorientation at liquid surfaces with time-resolved sum-frequency spectroscopy: a theoretical framework. *J. Phys. Chem. B* 113:7564–73
144. Bonn M, Bakker HJ, Ghosh A, Yamamoto S, Sovago M, et al. 2010. Structural inhomogeneity of interfacial water at lipid monolayers revealed by surface-specific vibrational pump-probe spectroscopy. *J. Am. Chem. Soc.* 132:14971–78
145. Wang H, Yan ECY, Borguet E, Eisenthal KB. 1996. Second harmonic generation from the surface of centrosymmetric particles in bulk solution. *Chem. Phys. Lett.* 259:15–20
146. Eisenthal KB. 2006. Second harmonic spectroscopy of aqueous nano- and microparticle interfaces. *Chem. Rev.* 106:1462–77
147. Roke S, Bonn M, Petukhov AV. 2004. Nonlinear optical scattering: the concept of effective susceptibility. *Phys. Rev. B* 70:115106
148. Roke S, Roeterdink WG, Wijnhoven J, Petukhov AV, Kleyn Aart W, et al. 2003. Vibrational sum frequency scattering from a submicron suspension. *Phys. Rev. Lett.* 91:258302

Annual Review of
Physical Chemistry
Volume 63, 2012

Contents

Indexes

Errata

An online log of corrections to Annual Review of Physical Chemistry chapters (if any, 1997 to the present) may be found at http://physchem.AnnualReviews.org/errata.shtml